



Article

The Apparent Tidal Decay of WASP-4 b Can Be Explained by the Rømer Effect

Jan-Vincent Harre *  and Alexis M. S. Smith 

Institute of Planetary Research, German Aerospace Center (DLR), Rutherfordstraße 2, 12489 Berlin, Germany; alexis.smith@dlr.de

* Correspondence: jan-vincent.harre@dlr.de

Abstract: Tidal orbital decay plays a vital role in the evolution of hot Jupiter systems. As of now, this has only been observationally confirmed for the WASP-12 system. There are a few other candidates, including WASP-4 b, but no conclusive result could be obtained for these systems as of yet. In this study, we present an analysis of new TESS data of WASP-4 b together with archival data, taking the light–time effect (LTE) induced by the second planetary companion into account as well. We make use of three different Markov chain Monte Carlo models: a circular orbit with a constant orbital period, a circular orbit with a decaying orbit, and an elliptical orbit with apsidal precession. This analysis is repeated for four cases. The first case features no LTE correction, with the remaining three cases featuring three different timing correction approaches because of the large uncertainties of the ephemeris of planet c. Comparison of these models yields no conclusive answer to the cause of WASP-4 b’s apparent transit timing variations. A broad range of values of the orbital decay and apsidal precession parameters are possible, depending on the LTE correction. However, the LTE caused by planet c can explain on its own—in full—the observed transit timing variations of planet b, with no orbital decay or apsidal precession being required at all. This work highlights the importance of continued photometric and spectroscopic monitoring of hot Jupiters.

Keywords: exoplanet evolution; exoplanet migration; tidal interaction; photometry; transits



Citation: Harre, J.-V.; Smith, A.M.S. The Apparent Tidal Decay of WASP-4 b Can Be Explained by the Rømer Effect. *Universe* **2023**, *9*, 506. <https://doi.org/10.3390/universe9120506>

Academic Editor: Tamás Borkovits

Received: 6 November 2023

Revised: 1 December 2023

Accepted: 3 December 2023

Published: 5 December 2023



Copyright: © 2023 by the authors. Licensee MDPI, Basel, Switzerland. This article is an open access article distributed under the terms and conditions of the Creative Commons Attribution (CC BY) license (<https://creativecommons.org/licenses/by/4.0/>).

1. Introduction

The study of exoplanets has unveiled a great diversity in terms of their physical properties, orbital characteristics, and formation mechanisms. Among the most intriguing exoplanet classes are the hot Jupiters. These relatively rare companions (e.g., [1]) stand out as a group of gas giants that orbit their host stars at exceptionally close distances and have challenged our understanding of planetary formation and evolution. One of the key phenomena that has piqued the interest of astronomers is the tidal orbital decay of hot Jupiters, and as of now only WASP-12 b could be observationally confirmed to experience this effect [2–4]. However, there seems to be evidence for the occurrence rates of hot Jupiters in orbit around Sun-like stars to decrease with stellar age, as opposed to the occurrence rates of cold Jupiters, as found by Miyazaki and Masuda [5]. This is supported by the likely observation of planetary engulfment by a Sun-like star made by the Zwicky Transient Facility [6].

Due to the close proximity of hot Jupiters to their stellar hosts, there are strong tidal interactions between the two bodies. These gravitational interactions can manifest themselves in the planet, raising a bulge on the surface of the star. Depending on the rotational period of the star and the planetary orbital period, the viscosity of the stellar plasma can lead to a lag between the position of the tidal bulge and the virtual line connecting the stellar and planetary centers. If the star is rotating slower than the planet is orbiting around it, the orbital angular momentum of the planet will be transferred to the star (equilibrium tide). The dynamical tide, arising from stellar oscillations, also contributes to this [7]. This means that the star will spin up, and the planetary orbit will shrink gradually [8,9]. This provides us with insights into the long-term stability of these systems.

WASP-4 b is a hot Jupiter discovered by Wilson et al. [10]. It shows TTVs that have been examined before, and other effects, mimicking the orbital decay signature, were ruled out previously, like the Applegate mechanism [11,12]. However, apsidal precession due to a small eccentricity of the planetary orbit, or TTVs arising from the Rømer effect (or light-time effect, LTE hereafter; Irwin [13]), due to a companion in the system, have not yet been ruled out as the cause of the TTVs, even after the discovery of the companion candidate. Previous studies examining the decay rate in the case of tidal orbital decay found values in the range from $-4.8 \text{ ms year}^{-1}$ to $-12.6 \text{ ms year}^{-1}$ [12,14–18], with the most recent estimate being $\dot{P} = (-6.2 \pm 1.2) \text{ ms year}^{-1}$ [19]. The differences between the measurements arise from the influence of additional timing data in each subsequent study.

In this work, we re-examine the TTVs in this system by making use of recently acquired TESS photometry and combine them with archival data from previous works. In particular, we account for the time-shift due to the LTE induced by the additional planet candidate, as discovered by Turner et al. [18]. The observations are described in Section 2, with our modeling and the results thereof being described in Sections 3 and 4, respectively. The latter are discussed in Section 5, and our final conclusions can be found in Section 6.

2. Observations

For our analysis, we made use of the previously described data set in Harre et al. [19] for WASP-4 b. In short, this data set is mainly based on the homogeneous re-analysis of previously published light curves from Baluev et al. [16], with the addition of TESS Sectors 28 and 29, as well as a re-analysis of the TESS Sector 2 data. Furthermore, in [19], we re-fitted the publicly available light curves from the ExoClock project [20] and from WASP [10] and added eight transit observations taken with the CHEOPS space telescope [21]. Included in this data set are also four occultation timings from the literature [22–24]. All these timings, including three different corrections, can be found in Appendix B, Table A1, for the transit timings and Table A2 for the occultation timings.

To this data set, we add new TESS observations from Sector 69 at a cadence of 120 s. We make use of the Presearch Data Conditioning Simple Aperture Photometry (PDCSAP) flux for the analysis of the light curves, which consists of data produced by the TESS Science Processing Operations Center (SPOC) at the NASA Ames Research Center [25]. These data are publicly available at MAST¹.

3. Modeling

3.1. Light Curve Modeling

For the analysis of the TESS transits, we made use of the Transit and Light Curve Modeler (TLCM, Csizmadia [26]), as described in Harre et al. [19]. In a first run, we fitted all transits together to obtain the combined shape of all transits to reduce the impact of stellar activity on the transit timings. The respective priors are shown in Table 1. During a second run, we fixed the shapes of the transits to those of the combined model and fitted all transits individually, with only the transit ephemerides being free. In both cases, we used the median solution for the final results.

Table 1. The resulting parameters from the TLCM fit to the TESS S69 data. The impact parameters are given by b , and u_a and u_b describe the quadratic limb-darkening parameters. T_0 is given in $[\text{BJD}_{\text{TDB}} - 2,450,000]$, and \mathcal{U} denotes a uniform prior.

Parameter (Unit)	Prior	Result
$a R_{\star}^{-1}$	$\mathcal{U}(5.4773 \pm 0.1000)$	5.39795 ± 0.01864
$R_p R_{\star}^{-1}$	$\mathcal{U}(0.1540 \pm 0.0100)$	0.1524 ± 0.0009
b	$\mathcal{U}(0.5 \pm 1.0)$	0.219 ± 0.015
P (d)	$\mathcal{U}(1.338231 \pm 0.000100)$	1.338239 ± 0.000014
T_0	$\mathcal{U}(10,192.575 \pm 0.050)$	$10,192.57567 \pm 0.00008$
u_a	$\mathcal{U}(0.5 \pm 1.0)$	0.35 ± 0.10
u_b	$\mathcal{U}(0.5 \pm 1.0)$	0.22 ± 0.14

3.2. Transit Timing Variation Analysis

For the analysis of the mid-transit times, obtained from our light curve modeling, we employ the same three models as Harre et al. [19]. The first is a model assuming a circular Keplerian orbit, describing a linear ephemeris with a constant orbital period:

$$t_{\text{tra}}(N) = T_0 + N P, \tag{1}$$

$$t_{\text{occ}}(N) = T_0 + \frac{P}{2} + N P, \tag{2}$$

where $t_{\text{tra}}(N)$ and $t_{\text{occ}}(N)$ are the calculated mid-transit and mid-occultation timings at the epoch N , T_0 denotes the reference mid-transit time, and P denotes the planetary orbital period. This gives us two free parameters in the fit.

The second model describes the case of a decaying orbit due to the transfer of angular momentum (see, e.g., Counselman [8], Rasio et al. [9]). These are quadratic functions with a constant change in the orbital period of the planet:

$$t_{\text{tra}}(N) = T_0 + N P + \frac{1}{2} \frac{dP}{dN} N^2, \tag{3}$$

$$t_{\text{occ}}(N) = T_0 + \frac{P}{2} + N P + \frac{1}{2} \frac{dP}{dN} N^2. \tag{4}$$

This constant change in the orbital period is denoted by the decay rate $\frac{dP}{dN}$, which can be converted to the period derivative $\dot{P} = \frac{dP}{dt} = \frac{1}{P} \frac{dP}{dN}$. There are three free parameters (T_0 , P , and $\frac{dP}{dN}$) when fitting this model. The period derivative is linked to the stellar tidal modified quality factor Q'_* via the constant-phase lag model, as defined in Goldreich and Soter [27]:

$$\dot{P} = f \frac{\pi}{Q'_*} \frac{M_p}{M_*} \left(\frac{R_*}{a} \right)^5, \tag{5}$$

where f denotes the tidal factor, M_p and M_* the planetary and stellar masses, R_* the stellar radius, and a the semi-major axis of the planetary orbit. Depending on the ratio of the planetary orbital period to the stellar rotational period and the orbital (mis-)alignment, f takes different values. If the planetary orbital period is shorter than the rotation period of the star, as is the case for WASP-4 b [28], we obtain $f = -\frac{27}{2}$. Refer to Section 4 of Harre et al. [19] for a more detailed description, which also includes the case of inclined orbits and different planet-to-star period ratios.

The third model we are using is an apsidal precession orbit, where a small eccentricity e leads the planetary orbit to precess around the star. This can, on relatively short timescales, induce the same TTV signature as orbital decay, which makes it hard to differentiate the two models if the orbital eccentricity is only loosely constrained. This sinusoidal model follows the descriptions of Giménez and Bastero [29]:

$$t_{\text{tra}}(N) = t_0 + N P_s - \frac{e P_a}{\pi} \cos \omega(N), \tag{6}$$

$$t_{\text{occ}}(N) = t_0 + \frac{P_a}{2} + N P_s + \frac{e P_a}{\pi} \cos \omega(N), \tag{7}$$

where P_s is the sidereal period, P_a the anomalistic period, and ω the argument of pericenter. The sidereal and anomalistic periods are related via the following:

$$P_s = P_a \left(1 - \frac{1}{2\pi} \frac{d\omega}{dN} \right), \tag{8}$$

with a constant change in the argument of pericenter $\frac{d\omega}{dN}$. The relationship between ω and N can be described as follows:

$$\omega(N) = \omega_0 + \frac{d\omega}{dN} N, \tag{9}$$

with ω_0 being the argument of pericenter at the reference time T_0 . In total, this model gives us five free parameters in the fitting process.

These three models are then fitted to the data via MCMC optimization using the *emcee Python* package [30]. Per model, we use 100 walkers and use a burn-in period of 10,000 steps with a total chain length of 75,000 steps. Convergence is ensured by checking that the chains are longer than 50 times the autocorrelation time of the parameters. The priors for our models can be found in Table 2.

Table 2. Priors and results from our MCMC modeling of the transit timings without any LTE correction. T_0 is given in $\text{BJD}_{\text{TDB}} - 2,450,000$. Units are given in parentheses if applicable. Priors were chosen according to the results of Harre et al. [19] with enough flexibility for the walkers to sufficiently explore the parameter space.

Model	Parameter	Prior	Result
Circular orbit	T_0	$\mathcal{U}(7000, 8000)$	7490.68717 ± 0.00002
	P (d)	$\mathcal{U}(1.3, 1.4)$	$1.33823133 \pm 0.00000001$
	BIC	-	382.45
Orbital decay	T_0	$\mathcal{U}(7000, 8000)$	7490.68735 ± 0.00002
	P (d)	$\mathcal{U}(1.3, 1.4)$	$1.33823122 \pm 0.00000001$
	dP/dN (d/orbit)	$\mathcal{U}(-10^{-8}, -10^{-11})$	$(-2.43 \pm 0.22) \times 10^{-10}$
	BIC	-	263.01
Apsidal precession	T_0	$\mathcal{U}(7000, 8000)$	7490.68690 ± 0.00019
	P (d)	$\mathcal{U}(1.3, 1.4)$	$1.33823140 \pm 0.00000009$
	$d\omega/dN$ (rad/orbit)	$\mathcal{U}(0.0001, 0.002)$	$(7.68 \pm 1.60) \times 10^{-4}$
	e	$\mathcal{U}(10^{-6}, 10^{-2})$	0.0013 ± 0.0005
	ω_0 (rad)	$\mathcal{U}(2, 2\pi)$	3.770 ± 0.242
	BIC	-	271.62

3.3. Light-Time Effect

The presence of a candidate planetary companion in a 7000 d orbit, as established by Turner et al. [18], would induce an orbital motion onto WASP-4. Due to the high mass of this candidate (“planet c” hereafter), the system’s center of mass is shifted by about 8.9 times the radius of WASP-4 (see Figure 1). This will have a significant impact on the observed mid-transit times because of the time difference that it takes the light to travel from the far side to the near side of the orbit from our point of view. In some cases, this could induce TTVs akin to the imprint of tidal decay on short timescales, depending on the orbital period of planet c. To include a correction of the LTE, we apply the formula of Schneider [31] to find the maximum time-shift from this effect for circular orbits:

$$\Delta T_{\text{max}} = 2 \frac{M_p}{M_\star} \frac{a \sin i}{c}, \tag{10}$$

where ΔT_{max} is the maximum resulting time-shift due to the LTE, i is the inclination of the planetary orbit, and c is the speed of light. For WASP-4, using the planetary parameters of planet c, and assuming a circular orbit with $i = 90^\circ$, we obtain a maximum time-shift of $\Delta T_{\text{max}} = 37.7$ s. To validate this result, we simulate the system using the N-body code *REBOUND* [32] and measure the orbit of the star around the system’s center of mass, as shown in Figure 1. From this, we obtain $\Delta T_{\text{max}} = 37.6$ s. Using the non-circular solution from Turner et al. [18] for planet c, we obtain $\Delta T_{\text{max,ell}} = 41.1$ s. However, since the non-

circular solution is not preferred in their paper, we adopt the circular solution and correct our transit times according to the following:

$$\Delta T(t) = \Delta T_{\max} \left(\frac{1}{2} \cos \left(2\pi \frac{t - T_{0,c}}{P_c} \right) + \frac{1}{2} \right), \quad (11)$$

where $\Delta T(t)$ is the time-shift due to the LTE at the time t , $T_{0,c}$ is the time of inferior conjunction of planet c , and $P_c = 7001.0$ d is the orbital period of planet c . This formula arises because the star is at its furthest point from us at the time of inferior conjunction of planet c . Due to the uncertainty of the time of conjunction of planet c ($T_{0,c} = 2,455,059^{+2300}_{-2100}$ d (BJD_{TDB})), we examine three cases of the LTE correction: firstly, assuming the best-fit value of the time of conjunction; secondly, the minimum value of the 1σ interval; and lastly, the maximum value of the 1σ interval.

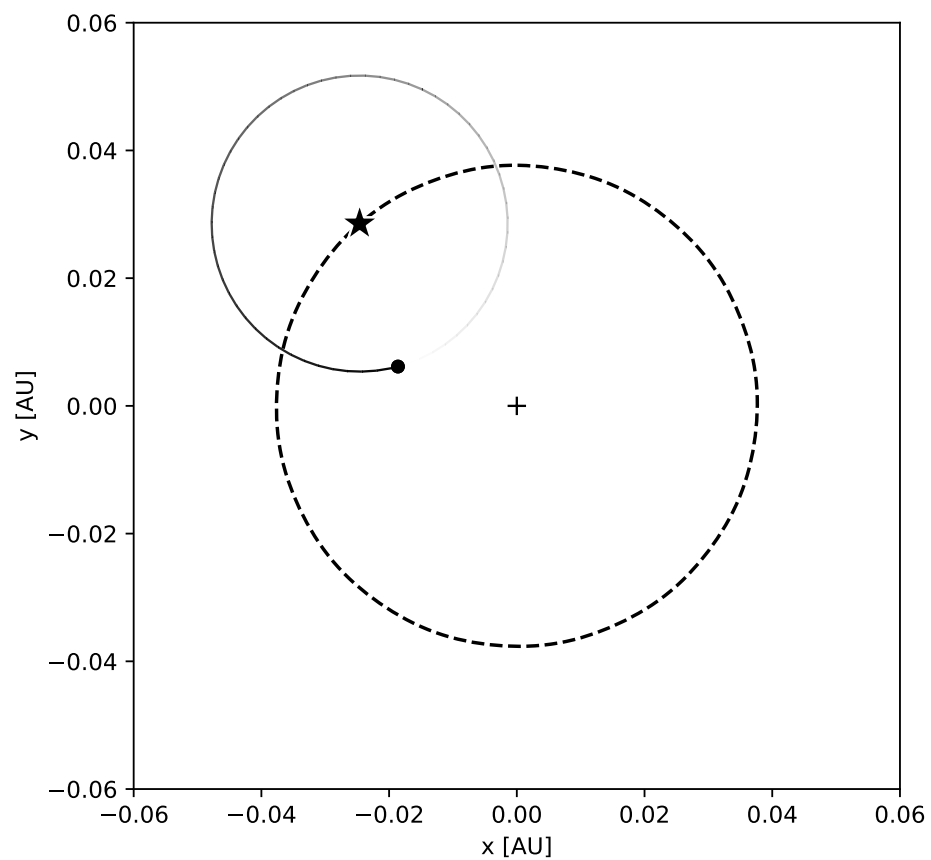


Figure 1. The orbits of WASP-4 (star symbol, dashed line) and WASP-4b (black dot, solid line) with reference to the system’s center of mass (black plus symbol) from *REBOUND*. The x - and y -axes lie within the orbital plane of the planets, which are assumed to be coplanar. The orbit of planet c is not visible in this view, since its semi-major axis is assumed to be 6.82 AU.

4. Results

4.1. Transit Fitting with *TLCM*

The priors for and results from the combined *TLCM* fit of all TESS transits from Sector 69 to constrain the transit shape are listed in Table 1, with the fit of the median model to the data shown in Figure 2. We find a root-mean-square scatter of 2.56 ppt between the data and our model. The resulting mid-transit times can be found in Table A1 in Appendix B.

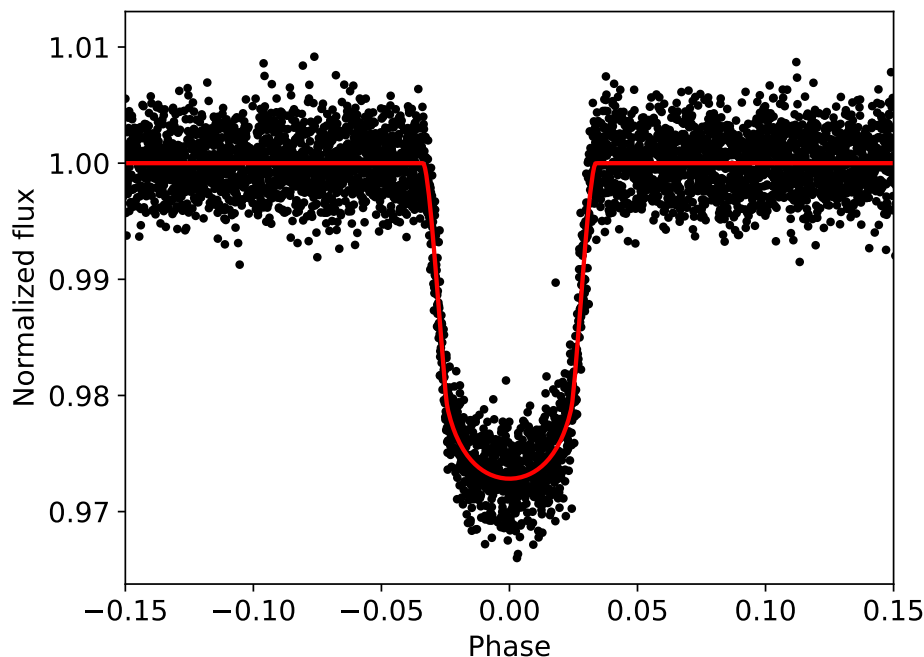


Figure 2. Phase-folded TESS light curve of WASP-4b from Sector 69, including 16 transits. The data are shown as black dots after modeling and correction with *TLCM*, with the median solution model shown as the red line.

4.2. TTV Fits without LTE Correction

The priors for the MCMC modeling of the circular orbit, orbital decay, and apsidal precession models and their resulting parameters are listed in Table 2.

We find an orbital decay rate of $\dot{P} = (-5.75 \pm 0.52) \text{ ms year}^{-1}$, leading to a stellar modified quality factor for WASP-4 of $Q'_* = (6.10 \pm 0.55) \times 10^4$ and a decay timescale of $\tau = (20.2 \pm 1.8) \text{ Myear}$ from the median solution. The BIC values of our solutions are obtained via the following calculation:

$$BIC = \chi^2 + k \cdot \ln(N), \tag{12}$$

with k being the number of free parameters and N the number of data points. For the orbital decay fit, we find $\Delta BIC_{\text{decay}} = 119.4$ between the linear and tidal decay models, in favor of the latter. In the case of apsidal precession, we find a precession rate of $\dot{\omega} = \frac{dw}{dt} = \frac{1}{P} \frac{dw}{dN} = (0.033 \pm 0.007)^\circ d^{-1}$ and a small eccentricity of $e = 0.0013 \pm 0.0005$. The fit yields $\Delta BIC_{\text{precession}} = 110.7$ between the linear and apsidal precession models. This leads to a difference of $\Delta BIC_{\text{dec.,prec.}} = 8.7$ in favor of the orbital decay model.

The result of the MCMC fit to the transit and occultation timing data including the final median models is shown in Figure 3. The latest data points highlight the deviation from a linear ephemeris in this system.

4.3. TTV Fits with LTE Correction

In case the candidate planet c does exist, we corrected for the induced LTE with a maximum time-shift of about 38 s in three different cases. These cases are (1) planet c has the best-fit time of inferior conjunction from model #3 of Turner et al. [18], (2) the time of inferior conjunction is at the lower boundary of the respective 1σ confidence interval, and (3) the time of inferior conjunction is at the upper boundary of the 1σ confidence interval. The corrections, according to Equation (11), are subtracted for each transit and occultation timing.

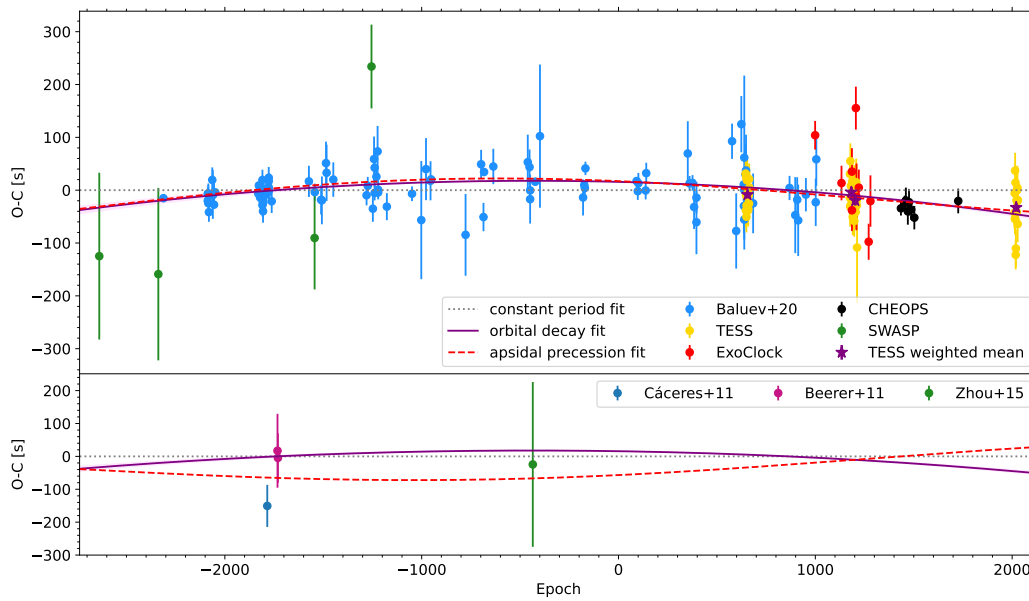


Figure 3. O-C plot showing all transit timing (**top**) and occultation data (**bottom**) together with the orbital decay and apsidal precession models. The transit number from the reference epoch is shown on the x-axis, while the deviation from the median linear ephemeris is shown on the y-axis. Colors are according to the legend, with the pink shaded area showing the 1σ interval around the median solution orbital decay fit. For the available TESS data, the weighted mean timings with their respective error bars for each sector have been added. No LTE correction was applied in this case.

The results in Table 3 show that the orbital decay model provides the best fit to the data in case (1), with the nominal LTE correction, although this model is only slightly preferred over the apsidal precession model. In this case, the decay rate would be $\dot{P} = (-7.04 \pm 0.52) \text{ ms year}^{-1}$, leading to $Q'_* = (4.98 \pm 0.37) \times 10^4$ and a decay time-scale of $\tau = (16.5 \pm 1.2) \text{ Myear}$. The apsidal precession model yields $\dot{\omega} = (0.024 \pm 0.007)^\circ \text{ d}^{-1}$ with an eccentricity of $e = 0.0029 \pm 0.0019$. This case is displayed in Figure 4.

In case (2), where the lower boundary of the 1σ interval of $T_{0,c}$ is used for the LTE correction, the apsidal precession model is preferred with a ΔBIC of 20 in comparison to the orbital decay model. The linear model is heavily disfavored. Assuming the orbital decay model to be true, we find an enhanced decay rate of $\dot{P} = (-9.35 \pm 0.52) \text{ ms year}^{-1}$, yielding $Q'_* = (3.75 \pm 0.21) \times 10^4$ and $\tau = (12.4 \pm 0.7) \text{ Myear}$. From the apsidal precession model, we obtain $\dot{\omega} = (0.041 \pm 0.005)^\circ \text{ d}^{-1}$ with $e = 0.0016 \pm 0.0003$. This case is shown in Appendix A, Figure A1.

Case (3), using the upper boundary of the time of inferior conjunction of planet c, shows that the orbital decay model provides the best fit to the data, with the circular orbit model fitting only slightly worse ($\Delta\text{BIC} < 3$), whereas the apsidal precession model fits worse with $\Delta\text{BIC} \approx 25 - 30$. In this case, the TTV signature is flattened due to the LTE correction. This results in a small decay rate of $\dot{P} = (-1.45 \pm 0.50) \text{ ms year}^{-1}$, leading to $Q'_* = (2.42 \pm 0.83) \times 10^5$ and $\tau = 80.2 \pm 27.7 \text{ Myear}$. In the apsidal precession case, we obtain $\dot{\omega} = (0.027 \pm 0.012)^\circ \text{ d}^{-1}$ with a small eccentricity of $e = 0.0010 \pm 0.0007$. The TTV models for this case are shown in Appendix A, Figure A2.

According to Turner et al. [18], the TTVs induced by planet c onto planet b should not exceed 2 s, which is why they are neglected here.

Table 3. Results from our MCMC modeling for the three cases of the LTE correction. The priors are the same as those given in Table 2. T_0 is given in $\text{BJD}_{\text{TDB}} - 2,450,000$. Units are given in parentheses if applicable. LTE refers to case (1), and LTE_{low} and LTE_{up} refer to cases (2) and (3), respectively. ΔBIC is defined relative to the circular Keplerian orbit case for each LTE correction. Note that the ΔBIC values should only be compared within a column, not between columns.

Model	Parameter	Result LTE	Result $\text{LTE}_{\text{lower}}$	Result $\text{LTE}_{\text{upper}}$
Circ. orbit	T_0	7490.68699 ± 0.00002	7490.68697 ± 0.00002	7490.68690 ± 0.00002
	P (d)	$1.33823145 \pm 0.00000001$	$1.33823129 \pm 0.00000001$	$1.33823126 \pm 0.00000001$
	ΔBIC	0	0	0
Orb. decay	T_0	7490.68721 ± 0.00002	7490.68727 ± 0.00002	7490.68695 ± 0.00002
	P (d)	$1.33823132 \pm 0.00000001$	$1.33823112 \pm 0.00000001$	$1.33823124 \pm 0.00000001$
	dP/dN (d/orbit)	$(-2.97 \pm 0.22) \times 10^{-10}$	$(-3.94 \pm 0.22) \times 10^{-10}$	$(-0.61 \pm 0.21) \times 10^{-10}$
	ΔBIC	-181.47	-323.87	-2.65
Aps. prec.	T_0	7490.68608 ± 0.00055	7490.68677 ± 0.000096	7490.68684 ± 0.00018
	P (d)	$1.33823113 \pm 0.00000026$	$1.33823141 \pm 0.00000008$	$1.33823142 \pm 0.00000013$
	$d\omega/dN$ (rad/orbit)	$(5.51 \pm 1.69) \times 10^{-4}$	$(9.69 \pm 1.16) \times 10^{-4}$	$(6.31 \pm 2.76) \times 10^{-4}$
	e	0.0029 ± 0.0019	0.0016 ± 0.0003	0.0010 ± 0.0007
	ω_0 (rad)	2.795 ± 0.274	3.922 ± 0.105	4.455 ± 0.515
	ΔBIC	-177.46	-343.83	+25.66

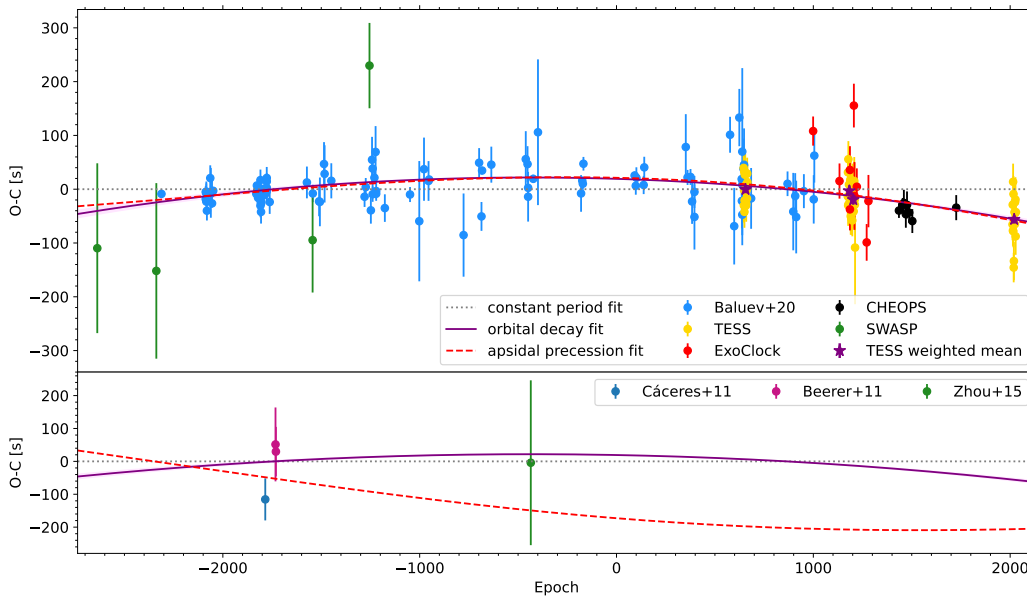


Figure 4. Same as Figure 3, but with the nominal LTE correction applied to the timing data to account for the influence of planet c.

5. Discussion

5.1. TTVs of WASP-4 b

As is evident from the results of our TTV modeling in Tables 2 and 3, the consideration of the LTE is very important in this system. The results of the orbital decay and apsidal precession modeling are only comparable to each other to a certain degree for the cases that were examined here.

If the detection of WASP-4 c should turn out spurious, then the measured decay rate value is comparable, albeit slightly smaller than those from previous studies [12,14–16,18,19,33]. In this case, the apsidal precession model would be disfavored by $\Delta\text{BIC} = 8.5$, which is a bit higher than in the latest study [19]. The decay rates are consistent within 1σ , with the eccentricity in the precession model being doubled, compared to the previous result, which is still in agreement with our value and uncertainty. The linear model is disfavored by $\Delta\text{BIC} \approx 110 - 120$.

The three different LTE corrections lead to three vastly different results. The nominal LTE correction agrees within 3σ with the results without the LTE correction for most of

the parameters. The other solutions do not. Depending on the correction, we obtain decay rates in the range from $(-9.35 \pm 0.52) \times 10^4 \text{ ms year}^{-1}$ to $(-1.45 \pm 0.50) \times 10^4 \text{ ms year}^{-1}$. This means that the LTE induced by a planetary companion can solely explain the observed TTVs. The quite broad range of results can only be further constrained with more radial velocity measurements to reduce the size of the error bars on the parameters of WASP-4 c. However, a value near the middle of this range is more probable. From these results, we obtain modified stellar quality factors in the range from 3.8×10^4 to 2.4×10^5 , which includes the value of $Q'_* = 1.8 \times 10^5$ obtained for WASP-12 b [2]. Moreover, this leads to decay timescales ranging from 12 Myear to 80 Myear. The apsidal precession models show a similar range of possible values, like the orbital decay models. However, with more observations, either transits or especially occultations, the models should be relatively easy to distinguish. Occultation observations with JWST, for example, could perform a double duty in this case. They can help to refine atmospheric properties and provide very accurate occultation timing measurements, which might be able to rule out either of the TTV models.

These results highlight the importance of continued radial velocity observations, even, or especially, in hot Jupiter systems. One theory of how hot Jupiters get into their tight orbits is high-eccentricity migration, which necessitates the presence of a massive second companion for the excitation of the high eccentricities that are required for this migration pathway [34,35]. Finding such a body requires long observational baselines due to the distance of the perturber to the host star.

5.2. Optimal Observing Strategy

For hot Jupiter systems in general, the most favorable tidal orbital decay systems have, according to Equation (5) and Table 2 in Harre et al. [19], first and foremost with the highest impact, large stellar radii and short orbital separations. Small stellar tidal quality factors, high planetary masses, and low stellar masses are also beneficial. However, stellar tidal quality factors can only be constrained after the observations. Furthermore, orbital periods of the companion bodies smaller than the stellar rotation periods are essential, but this only applies to equatorial orbits. For polar orbits, orbital decay should always be present, even for fast-rotating stars. Still, slow stellar rotation rates are beneficial here as well. In summary, as is known, hot Jupiters are prime targets to examine the effect of tidal orbital decay. Moreover, brown dwarfs on close-in orbits should even experience a more pronounced effect due to their higher masses. In addition, companions orbiting evolved or (sub-)giant stars should present the best laboratories to explore orbital decay. Yet, the expected lifetimes of these close-by companions will be relatively short, and observing them is only possible in just the right time window, providing us with only a very small sample of targets (see, e.g., Grunblatt et al. [36]).

In terms of radial velocity monitoring, after sufficient data have been accumulated for the characterization of hot Jupiters, it would be optimal for the target to be re-observed every few months so that even farther out companions could be detected in principle. This would shed light not only onto the architecture of these systems but also on their formation and migration pathways. This case study is an excellent example of this, where an outer companion candidate has been detected [18], but the whole detection hinges on the latest set of observations not being spurious or having an incorrect offset in relation to the previously accumulated RV data. Due to the possibility for the outer planet to induce a small eccentricity onto the orbit of the inner planet, a non-detection constraining possible planet masses and distances from the host star could rule out the apsidal precession models in some cases. This could be achieved by comparing the eccentricity damping timescale to the orbital decay timescale.

For photometric observations, it would be ideal to obtain high-precision transit observations every few months. Long-term monitoring is essential to detect orbital decay signatures with a baseline of more than 15 years having been necessary for WASP-12 b [2]. Occultation observations would be even more helpful to differentiate the orbital decay and apsidal precession models, not only from the point-of-view of TTV fitting but also

because they can indicate eccentricities directly. In addition to the timing, secondary eclipse observations can give clues about the atmospheric composition or the thermal structure of the atmosphere and the presence of clouds (see, e.g., Jackson et al. [37], Scandariato et al. [38], van Sluijs et al. [39], Shi et al. [40], Hoyer et al. [41]).

The PLATO mission [42] has the potential to revolutionize the field with its long, uninterrupted observations. Due to the expected excellent precision of the observations, occultations of hot Jupiters are likely to be detected as well. This should allow discrimination between the orbital decay and apsidal precession models. In addition, even relatively far-out companions could be detected with radial velocity follow-up from PLATO's ground segment, should they not transit the host star. As well as PLATO, ESA's Gaia mission [43], starting with its fourth data release, has the potential to improve our understanding of already known hot Jupiter systems. Its precise astrometric measurements will allow for the detection of giant companions in these systems and provide detailed characterization of their orbits. This will provide information on the formation and migration history of each system.

6. Conclusions

By analyzing new TESS observations of WASP-4 in combination with archival timing data and taking into account the additional planet candidate in the system, we obtain a broad range of results for the cause of the TTVs of WASP-4 b. We examined a total of four cases. The first case does not take into account the presence of planet c and yields comparable results to the hitherto published results for this system in terms of the orbital decay parameters. In addition, the remaining cases consider, for the first time, the light–time effect from the host star's orbital motion around the system's center of mass, induced by planet c. Depending on the application of the timing correction, we find results that range from a slight preference ($\Delta\text{BIC} \approx 4$) of the orbital decay model in the nominal case (using the nominal value for the time of inferior conjunction of planet c from Turner et al. [18]), over a strong preference ($\Delta\text{BIC} \approx 20$) of the apsidal precession model using the lower boundary of the respective 1σ confidence interval, to a nearly indistinguishable result between the linear ephemeris and orbital decay models ($\Delta\text{BIC} \approx 2$) using the upper boundary of the respective interval for the time of inferior conjunction of planet c. These results leave us with no conclusive answer to the question of what the true origin of the TTVs of WASP-4 b is. We need more radial velocity observations to better constrain the phase of planet c. Only then will we be able to determine whether the LTE solely explains the observed TTVs, or whether other mechanisms, like tidal decay or apsidal precession, are present. It is, however, possible for it to be a mix of all of the effects mentioned here.

This case study highlights the importance of continued monitoring of hot Jupiter systems, in terms of photometric and radial velocity measurements. Only in this way can small effects, like orbital decay or apsidal precession, be measured and differentiated. An additional benefit is given by the chance of discovering and characterizing companions to hot Jupiters, providing hints of the formation and migration scenarios that lead to these special systems. This is a necessary step to inform our theoretical models of planet formation and migration and towards the final answer to the question of the origin of these planets.

Author Contributions: Formal analysis, J.-V.H.; writing—original draft preparation, J.-V.H.; writing—review and editing, A.M.S.S.; supervision, A.M.S.S.; funding acquisition, A.M.S.S. All authors have read and agreed to the published version of the manuscript.

Funding: This research was funded by the DFG priority program SPP 1992 “Exploring the Diversity of Extrasolar Planets (SM 486/2-1)”.

Data Availability Statement: The data underlying this article are available in Appendix B.

Acknowledgments: We thank the referees for their helpful comments and suggestions. This paper includes data collected with the TESS mission, obtained from the MAST data archive at the Space Telescope Science Institute (STScI). Funding for the TESS mission is provided by the NASA Explorer Program. STScI is operated by the Association of Universities for Research in Astronomy, Inc.,

under NASA contract NAS 5–26555. This work made use of Astropy:² a community-developed core Python package and an ecosystem of tools and resources for astronomy [44–46].

Conflicts of Interest: The authors declare no conflict of interest.

Appendix A. TTV Fits with LTE Correction

The TTV fits with the LTE correction at the lower and upper boundaries of the 1σ interval of the ephemeris of planet c from Turner et al. [18] are shown in Figures A1 and A2.

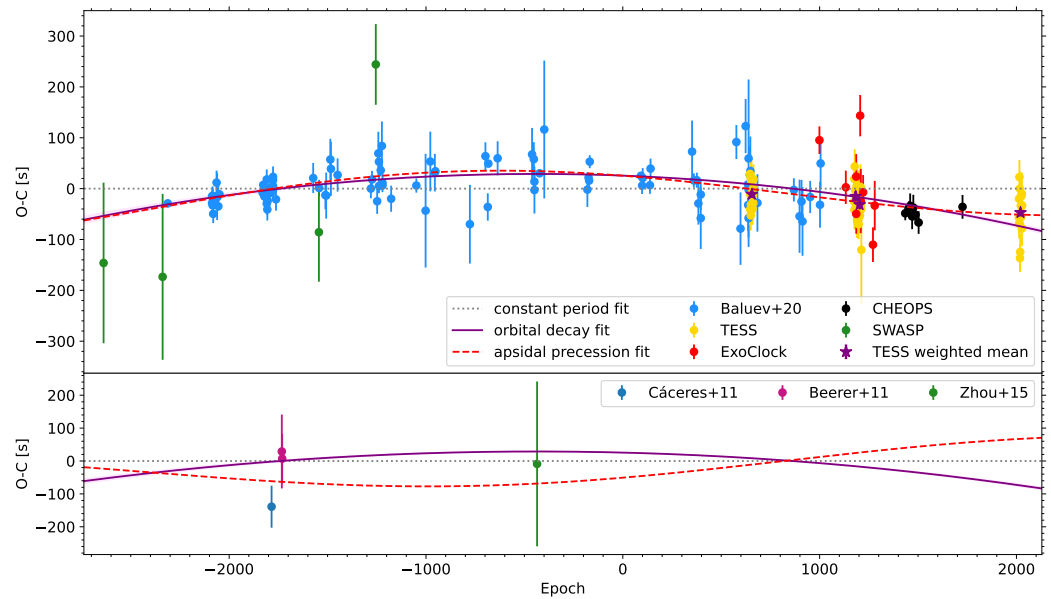


Figure A1. Same as Figure 3, but with the LTE correction applied to the timing data, using the lower limit of the 1σ interval of the time of inferior conjunction of planet c.

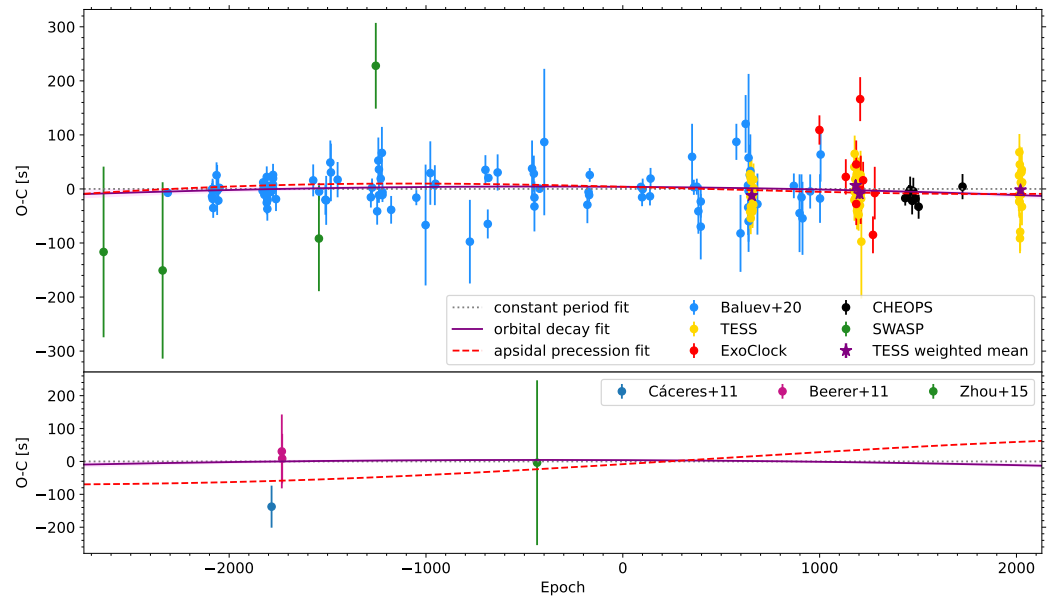


Figure A2. Same as Figure 3, but with the LTE correction, using the upper limit of the 1σ interval around the nominal time of inferior conjunction of planet c, applied to the timing data.

Appendix B. Transit and Occultation Timings

The transit and occultation timings of WASP-4 b, including those with the different LTE corrections, are given in Tables A1 and A2.

Table A1. Transit timings of WASP-4 b including three different corrections for the LTE. Time is given in $\text{BJD}_{\text{TDB}} - 2,450,000$. “Time” denotes the mid-transit times without any light–time correction. “Time LTE” denotes LTE-corrected timings using the nominal value for the time of inferior conjunction of planet c from Turner et al. [18], “Time $\text{LTE}_{\text{lower}}$ ” denotes the timings corrected using the lower boundary of the respective 1σ interval. “ $\text{LTE}_{\text{upper}}$ ” denotes the timings corrected using the upper boundary of the interval. The “Source” column denotes the source of the timings, with 0–4 defined as the homogeneous reanalysis from Baluev et al. [16] (0), TESS timings (1) from [19] and this work (last sector), and the ExoClock project (2) [20] as fitted by Harre et al. [19], as well as their CHEOPS timings (3), and WASP timings (4), respectively.

Time	Time LTE	Time $\text{LTE}_{\text{lower}}$	Time $\text{LTE}_{\text{upper}}$	Error (d)	Epoch	Source
3960.431480	3960.431143	3960.431479	3960.431127	0.001827	−305	4
4361.900484	4361.900090	4361.900463	4361.900200	0.001889	−5	4
4396.696163	4396.695765	4396.696138	4396.695885	0.000085	21	0
4697.798154	4697.797730	4697.798095	4697.797934	0.000063	246	0
4697.798306	4697.797882	4697.798247	4697.798086	0.000133	246	0
4701.813010	4701.812586	4701.812951	4701.812791	0.000217	249	0
4701.812980	4701.812556	4701.812921	4701.812761	0.000206	249	0
4701.812795	4701.812371	4701.812736	4701.812576	0.000148	249	0
4705.827294	4705.826869	4705.827234	4705.827075	0.000210	252	0
4728.577932	4728.577506	4728.577869	4728.577718	0.000274	269	0
4732.592308	4732.591883	4732.592245	4732.592095	0.000536	272	0
4732.592291	4732.591865	4732.592227	4732.592078	0.000145	272	0
4740.621727	4740.621301	4740.621663	4740.621516	0.000264	278	0
4740.621472	4740.621046	4740.621407	4740.621260	0.000093	278	0
4748.651131	4748.650704	4748.651065	4748.650921	0.000056	284	0
5041.723762	5041.723326	5041.723650	5041.723608	0.000121	503	0
5045.738636	5045.738201	5045.738523	5045.738483	0.000041	506	0
5049.753225	5049.752790	5049.753112	5049.753073	0.000042	509	0
5053.767759	5053.767324	5053.767646	5053.767608	0.000078	512	0
5069.826919	5069.826484	5069.826803	5069.826771	0.000226	524	0
5069.826367	5069.825932	5069.826251	5069.826219	0.000249	524	0
5069.826591	5069.826156	5069.826475	5069.826443	0.000227	524	0
5069.826740	5069.826305	5069.826624	5069.826592	0.000221	524	0
5069.826491	5069.826056	5069.826374	5069.826342	0.000128	524	0
5073.840928	5073.840493	5073.840811	5073.840781	0.000251	527	0
5073.841150	5073.840715	5073.841033	5073.841003	0.000232	527	0
5073.841110	5073.840675	5073.840993	5073.840963	0.000168	527	0
5073.841123	5073.840688	5073.841006	5073.840976	0.000209	527	0
5096.591358	5096.590923	5096.591237	5096.591215	0.000148	544	0
5100.605932	5100.605497	5100.605810	5100.605789	0.000101	547	0
5112.650371	5112.649936	5112.650247	5112.650230	0.000236	556	0
5112.650296	5112.649861	5112.650172	5112.650156	0.000177	556	0
5112.650162	5112.649727	5112.650038	5112.650021	0.000207	556	0
5112.650086	5112.649651	5112.649962	5112.649945	0.000261	556	0
5132.723325	5132.722891	5132.723198	5132.723188	0.000257	571	0
5385.649482	5385.649056	5385.649307	5385.649388	0.000342	760	0
5424.456950	5424.456526	5424.456768	5424.456862	0.001127	789	4
5425.796186	5425.795762	5425.796004	5425.796099	0.000188	790	0
5468.619420	5468.618999	5468.619229	5468.619339	0.000320	822	0
5473.972334	5473.971913	5473.972142	5473.972254	0.000524	826	0
5502.076007	5502.075589	5502.075810	5502.075932	0.000471	847	0
5506.090489	5506.090071	5506.090291	5506.090414	0.000616	850	0
5551.590205	5551.589791	5551.589999	5551.590137	0.000378	884	0

Table A1. Cont.

Time	Time LTE	Time LTE _{lower}	Time LTE _{upper}	Error (d)	Epoch	Source
5777.750955	5777.750564	5777.750705	5777.750916	0.000220	1053	0
5785.780551	5785.780160	5785.780299	5785.780512	0.000196	1059	0
5811.209560	5811.209172	5811.209303	5811.209524	0.000918	1078	4
5820.574064	5820.573678	5820.573805	5820.574029	0.000286	1085	0
5828.604540	5828.604155	5828.604280	5828.604506	0.000493	1091	0
5832.618492	5832.618107	5832.618231	5832.618458	0.000163	1094	0
5832.619044	5832.618660	5832.618783	5832.619011	0.000426	1094	0
5844.662930	5844.662547	5844.662667	5844.662898	0.000138	1103	0
5852.692871	5852.692489	5852.692606	5852.692840	0.000557	1109	0
5856.706724	5856.706342	5856.706458	5856.706693	0.000210	1112	0
5856.706666	5856.706284	5856.706400	5856.706635	0.000098	1112	0
5915.588533	5915.588159	5915.588257	5915.588508	0.000297	1156	0
6086.882427	6086.882078	6086.882118	6086.882414	0.000162	1284	0
6149.778721	6149.778382	6149.778402	6149.778713	0.001294	1331	0
6181.897390	6181.897056	6181.897065	6181.897383	0.000680	1355	0
6212.676454	6212.676126	6212.676124	6212.676449	0.000428	1378	0
6216.691180	6216.690852	6216.690849	6216.691175	0.000067	1381	0
6450.880446	6450.880160	6450.880079	6450.880446	0.000895	1556	0
6556.602268	6556.602001	6556.601887	6556.602267	0.000315	1635	0
6572.659887	6572.659624	6572.659504	6572.659886	0.000311	1647	0
6576.675568	6576.675305	6576.675184	6576.675567	0.000055	1650	0
6639.572561	6639.572310	6639.572170	6639.572558	0.000388	1697	0
6873.763138	6873.762933	6873.762724	6873.763123	0.000602	1872	0
6885.807112	6885.806910	6885.806696	6885.807096	0.000386	1881	0
6889.821295	6889.821093	6889.820879	6889.821279	0.000198	1884	0
6889.821104	6889.820902	6889.820688	6889.821088	0.000535	1884	0
6924.615500	6924.615305	6924.615081	6924.615481	0.000086	1910	0
6956.734051	6956.733862	6956.733630	6956.734030	0.001568	1934	0
7249.805368	7249.805234	7249.804933	7249.805315	0.000394	2153	0
7257.835029	7257.834897	7257.834595	7257.834976	0.000082	2159	0
7261.849657	7261.849525	7261.849222	7261.849603	0.000129	2162	0
7265.864781	7265.864650	7265.864347	7265.864726	0.000147	2165	0
7613.804649	7613.804575	7613.804219	7613.804542	0.000084	2425	0
7621.833815	7621.833742	7621.833385	7621.833706	0.000191	2431	0
7625.848681	7625.848609	7625.848252	7625.848572	0.000226	2434	0
7675.363083	7675.363018	7675.362656	7675.362966	0.000196	2471	0
7679.378156	7679.378091	7679.377730	7679.378038	0.000228	2474	0
7961.745397	7961.745366	7961.744993	7961.745227	0.000707	2685	0
7973.788824	7973.788795	7973.788421	7973.788652	0.000162	2694	0
7993.862304	7993.862276	7993.861903	7993.862128	0.000172	2709	0
8004.567627	8004.567600	8004.567227	8004.567449	0.000481	2717	0
8020.626070	8020.626045	8020.625672	8020.625890	0.000702	2729	0
8020.626608	8020.626583	8020.626210	8020.626427	0.000345	2729	0
8262.847714	8262.847706	8262.847347	8262.847486	0.000387	2910	0
8290.948607	8290.948600	8290.948243	8290.948373	0.000824	2931	0
8325.744960	8325.744955	8325.744601	8325.744720	0.000617	2957	0
8341.802413	8341.802409	8341.802057	8341.802170	0.000361	2969	0
8343.140176	8343.140171	8343.139820	8343.139932	0.000591	2970	0
8345.816340	8345.816336	8345.815985	8345.816096	0.000657	2972	0
8345.817698	8345.817694	8345.817343	8345.817454	0.001797	2972	0
8345.816987	8345.816983	8345.816632	8345.816743	0.000103	2972	0
8349.831750	8349.831747	8349.831396	8349.831506	0.000212	2975	0
8353.846717	8353.846713	8353.846363	8353.846471	0.000650	2978	0
8357.861497	8357.861493	8357.861144	8357.861251	0.000783	2981	0
8357.861077	8357.861073	8357.860723	8357.860830	0.000105	2981	0
8406.037105	8406.037103	8406.036759	8406.036849	0.000654	3017	0

Table A1. *Cont.*

Time	Time LTE	Time LTE _{lower}	Time LTE _{upper}	Error (d)	Epoch	Source
8355.184967	8355.184963	8355.184613	8355.184721	0.000330	2979	1
8356.522391	8356.522388	8356.522038	8356.522145	0.000367	2980	1
8357.860950	8357.860947	8357.860597	8357.860704	0.000316	2981	1
8359.199579	8359.199576	8359.199226	8359.199333	0.000311	2982	1
8360.536947	8360.536944	8360.536594	8360.536700	0.000343	2983	1
8361.875428	8361.875424	8361.875075	8361.875180	0.000307	2984	1
8363.214209	8363.214205	8363.213856	8363.213961	0.000361	2985	1
8364.551875	8364.551871	8364.551522	8364.551627	0.000348	2986	1
8365.890728	8365.890725	8365.890376	8365.890480	0.000393	2987	1
8369.905146	8369.905143	8369.904795	8369.904898	0.000361	2990	1
8371.242934	8371.242931	8371.242583	8371.242685	0.000310	2991	1
8372.581201	8372.581198	8372.580850	8372.580952	0.000384	2992	1
8373.919748	8373.919745	8373.919397	8373.919499	0.000348	2993	1
8375.257960	8375.257957	8375.257609	8375.257710	0.000319	2994	1
8376.596324	8376.596321	8376.595974	8376.596074	0.000336	2995	1
8377.934241	8377.934238	8377.933891	8377.933991	0.000352	2996	1
8379.273009	8379.273006	8379.272659	8379.272759	0.000344	2997	1
8380.611058	8380.611055	8380.610708	8380.610807	0.000374	2998	1
8653.610237	8653.610237	8653.609933	8653.609935	0.000265	3202	0
8692.418351	8692.418350	8692.418054	8692.418042	0.000833	3231	0
8705.801002	8705.801000	8705.800708	8705.800691	0.000492	3241	0
8712.491707	8712.491705	8712.491413	8712.491394	0.000782	3246	0
8764.683292	8764.683288	8764.683008	8764.682971	0.000366	3285	0
8827.581466	8827.581460	8827.581194	8827.581134	0.000314	3332	2
8831.594691	8831.594684	8831.594420	8831.594358	0.000521	3335	0
8835.610326	8835.610320	8835.610056	8835.609993	0.000581	3338	0
9006.903416	9006.903399	9006.903179	9006.903056	0.000379	3466	2
9063.108812	9063.108790	9063.108585	9063.108444	0.000397	3508	1
9064.447561	9064.447539	9064.447335	9064.447192	0.000362	3509	1
9065.785080	9065.785058	9065.784854	9065.784711	0.000439	3510	1
9067.124306	9067.124284	9067.124080	9067.123937	0.000390	3511	1
9068.461570	9068.461548	9068.461345	9068.461201	0.000417	3512	1
9069.799976	9069.799954	9069.799751	9069.799607	0.000463	3513	1
9071.138455	9071.138432	9071.138230	9071.138085	0.000530	3514	1
9076.491113	9076.491090	9076.490889	9076.490743	0.000431	3518	1
9077.829080	9077.829057	9077.828856	9077.828709	0.000453	3519	2
9077.829928	9077.829905	9077.829704	9077.829557	0.000511	3519	2
9077.829278	9077.829255	9077.829054	9077.828908	0.000418	3519	1
9079.167681	9079.167658	9079.167458	9079.167310	0.000403	3520	1
9080.506153	9080.506130	9080.505930	9080.505782	0.000467	3521	1
9081.844421	9081.844397	9081.844198	9081.844050	0.000441	3522	1
9083.181857	9083.181834	9083.181635	9083.181486	0.000398	3523	1
9084.520535	9084.520512	9084.520313	9084.520164	0.000599	3524	1
9088.534731	9088.534707	9088.534509	9088.534359	0.000346	3527	1
9089.873673	9089.873649	9089.873452	9089.873301	0.000309	3528	1
9091.211733	9091.211709	9091.211512	9091.211361	0.000347	3529	1
9092.549788	9092.549764	9092.549568	9092.549416	0.000379	3530	1
9093.887619	9093.887595	9093.887399	9093.887247	0.000341	3531	1
9095.226017	9095.225992	9095.225796	9095.225644	0.000364	3532	1
9096.564853	9096.564829	9096.564633	9096.564481	0.000453	3533	1
9097.902814	9097.902789	9097.902594	9097.902441	0.000368	3534	1

Table A1. *Cont.*

Time	Time LTE	Time LTE _{lower}	Time LTE _{upper}	Error (d)	Epoch	Source
9103.255438	9103.255413	9103.255219	9103.255064	0.000366	3538	1
9104.594195	9104.594169	9104.593976	9104.593821	0.000334	3539	1
9104.595944	9104.595919	9104.595726	9104.595570	0.000471	3539	2
9105.932501	9105.932475	9105.932283	9105.932127	0.000440	3540	1
9107.270785	9107.270759	9107.270567	9107.270410	0.000515	3541	1
9108.608905	9108.608879	9108.608687	9108.608530	0.000499	3542	1
9108.608695	9108.608669	9108.608477	9108.608321	0.000731	3542	2
9109.946842	9109.946816	9109.946625	9109.946467	0.000361	3543	1
9111.284969	9111.284943	9111.284752	9111.284594	0.000350	3544	1
9112.622279	9112.622253	9112.622062	9112.621904	0.001219	3545	1
9124.667672	9124.667644	9124.667457	9124.667295	0.000395	3554	2
9191.578053	9191.578019	9191.577852	9191.577668	0.000395	3604	2
9203.623026	9203.622991	9203.622827	9203.622639	0.000563	3613	2
9411.048723	9411.048663	9411.048564	9411.048314	0.000158	3768	3
9436.475245	9436.475181	9436.475090	9436.474834	0.000150	3787	3
9444.504679	9444.504614	9444.504526	9444.504267	0.000282	3793	3
9457.886752	9457.886685	9457.886602	9457.886339	0.000291	3803	3
9465.916342	9465.916274	9465.916193	9465.915928	0.000290	3809	3
9480.636724	9480.636653	9480.636577	9480.636308	0.000219	3820	3
9502.048249	9502.048175	9502.048106	9502.047832	0.000257	3836	3
9800.474200	9800.474078	9800.474109	9800.473767	0.000270	4059	3
10,183.208105	10,183.207912	10,183.208066	10,183.207674	0.000341	4345	1
10,184.546761	10,184.546568	10,184.546722	10,184.546330	0.000307	4346	1
10,185.884435	10,185.884242	10,185.884396	10,185.884004	0.000325	4347	1
10,187.223718	10,187.223524	10,187.223680	10,187.223287	0.000391	4348	1
10,188.560885	10,188.560691	10,188.560847	10,188.560454	0.000344	4349	1
10,189.899918	10,189.899724	10,189.899880	10,189.899488	0.000386	4350	1
10,191.236568	10,191.236374	10,191.236530	10,191.236138	0.000318	4351	1
10,192.574939	10,192.574744	10,192.574901	10,192.574509	0.000410	4352	1
10,196.590687	10,196.590492	10,196.590650	10,196.590257	0.000295	4355	1
10,197.929131	10,197.928935	10,197.929094	10,197.928701	0.000376	4356	1
10,199.266892	10,199.266696	10,199.266855	10,199.266462	0.000348	4357	1
10,200.605601	10,200.605405	10,200.605564	10,200.605171	0.000352	4358	1
10,201.943596	10,201.943399	10,201.943559	10,201.943166	0.000314	4359	1
10,203.282118	10,203.281921	10,203.282081	10,203.281688	0.000479	4360	1
10,204.619557	10,204.619360	10,204.619521	10,204.619127	0.000398	4361	1
10,205.958311	10,205.958114	10,205.958275	10,205.957881	0.000370	4362	1

Table A2. Occultation timings of WASP-4 b including three different corrections for the LTE. Time is given in $\text{BJD}_{\text{TDB}} - 2,450,000$. “Time” denotes the mid-occultation times without the light-time correction due to planet c, “Time LTE” denotes LTE-corrected timings using the nominal value for the time of inferior conjunction of planet c from Turner et al. [18], “Time LTE_{lower}” denotes the timings corrected using the lower boundary of the respective 1σ interval, and “LTE_{upper}” denotes the timings corrected using the upper boundary of the interval. The “Source” column denotes the source of the timings, with (5) the timing from Cáceres et al. [22], (6) the two from Beerer et al. [23], and (7) the one from Zhou et al. [24].

Time	Time LTE	Time LTE _{lower}	Time LTE _{upper}	Error (d)	Epoch	Source
5102.611620	5102.611185	5102.611498	5102.611478	0.000740	548.5	5
5172.201590	5172.201156	5172.201456	5172.201460	0.001300	600.5	6
5174.877800	5174.877366	5174.877665	5174.877671	0.000870	602.5	6
6907.887140	6907.886942	6907.886723	6907.887123	0.002900	1897.5	7

Notes

- ¹ <https://mast.stsci.edu/>, (accessed on 13 October 2023)
- ² <http://www.astropy.org>, (accessed on 15 October 2023)

References

1. Beleznyay, M.; Kunimoto, M. Exploring the dependence of hot Jupiter occurrence rates on stellar mass with TESS. *Mon. Not. RAS* **2022**, *516*, 75–83. [[CrossRef](#)]
2. Yee, S.W.; Winn, J.N.; Knutson, H.A.; Patra, K.C.; Vissapragada, S.; Zhang, M.M.; Holman, M.J.; Shporer, A.; Wright, J.T. The Orbit of WASP-12b Is Decaying. *Astrophys. J. Lett.* **2020**, *888*, L5. [[CrossRef](#)]
3. Turner, J.D.; Ridden-Harper, A.; Jayawardhana, R. Decaying Orbit of the Hot Jupiter WASP-12b: Confirmation with TESS Observations. *Astron. J.* **2021**, *161*, 72. [[CrossRef](#)]
4. Wong, I.; Shporer, A.; Vissapragada, S.; Greklek-McKeon, M.; Knutson, H.A.; Winn, J.N.; Benneke, B. TESS Revisits WASP-12: Updated Orbital Decay Rate and Constraints on Atmospheric Variability. *Astron. J.* **2022**, *163*, 175. [[CrossRef](#)]
5. Miyazaki, S.; Masuda, K. Evidence that the Occurrence Rate of Hot Jupiters around Sun-like Stars Decreases with Stellar Age. *arXiv* **2023**, arXiv:2309.14605. [[CrossRef](#)].
6. De, K.; MacLeod, M.; Karambelkar, V.; Jencson, J.E.; Chakrabarty, D.; Conroy, C.; Dekany, R.; Eilers, A.C.; Graham, M.J.; Hillenbrand, L.A.; et al. An infrared transient from a star engulfing a planet. *Nature* **2023**, *617*, 55–60. [[CrossRef](#)] [[PubMed](#)]
7. Ogilvie, G.I. Tidal Dissipation in Stars and Giant Planets. *Annu. Rev. Astron Astrophys.* **2014**, *52*, 171–210. [[CrossRef](#)]
8. Counselman, C.C., III. Outcomes of Tidal Evolution. *Astrophys. J.* **1973**, *180*, 307–316. [[CrossRef](#)]
9. Rasio, F.A.; Tout, C.A.; Lubow, S.H.; Livio, M. Tidal Decay of Close Planetary Orbits. *Astrophys. J.* **1996**, *470*, 1187. [[CrossRef](#)]
10. Wilson, D.M.; Gillon, M.; Hellier, C.; Maxted, P.F.L.; Pepe, F.; Queloz, D.; Anderson, D.R.; Collier Cameron, A.; Smalley, B.; Lister, T.A.; et al. WASP-4b: A 12th Magnitude Transiting Hot Jupiter in the Southern Hemisphere. *Astrophys. J. Lett.* **2008**, *675*, L113. [[CrossRef](#)]
11. Watson, C.A.; Marsh, T.R. Orbital period variations of hot Jupiters caused by the Applegate effect. *Mon. Not. RAS* **2010**, *405*, 2037–2043. [[CrossRef](#)]
12. Southworth, J.; Dominik, M.; Jørgensen, U.G.; Andersen, M.I.; Bozza, V.; Burgdorf, M.J.; D’Ago, G.; Dib, S.; Figuera Jaimes, R.; Fujii, Y.I.; et al. Transit timing variations in the WASP-4 planetary system. *Mon. Not. RAS* **2019**, *490*, 4230–4236. [[CrossRef](#)]
13. Irwin, J.B. The Determination of a Light-Time Orbit. *Astrophys. J.* **1952**, *116*, 211. [[CrossRef](#)]
14. Bouma, L.G.; Winn, J.N.; Baxter, C.; Bhatti, W.; Dai, F.; Daylan, T.; Désert, J.M.; Hill, M.L.; Kane, S.R.; Stassun, K.G.; et al. WASP-4b Arrived Early for the TESS Mission. *Astron. J.* **2019**, *157*, 217. [[CrossRef](#)]
15. Baluev, R.V.; Sokov, E.N.; Jones, H.R.A.; Shaidulin, V.S.; Sokova, I.A.; Nielsen, L.D.; Benni, P.; Schneider, E.M.; Villarreal D’Angelo, C.; Fernández-Lajús, E.; et al. Homogeneously derived transit timings for 17 exoplanets and reassessed TTV trends for WASP-12 and WASP-4. *Mon. Not. RAS* **2019**, *490*, 1294–1312. [[CrossRef](#)]
16. Baluev, R.V.; Sokov, E.N.; Hoyer, S.; Huitson, C.; da Silva, J.A.R.S.; Evans, P.; Sokova, I.A.; Knight, C.R.; Shaidulin, V.S. WASP-4 transit timing variation from a comprehensive set of 129 transits. *Mon. Not. RAS* **2020**, *496*, L11–L15. [[CrossRef](#)]
17. Maciejewski, G. Search for Planets in Hot Jupiter Systems with Multi-Sector TESS Photometry. II. Constraints on Planetary Companions in 12 Systems. *Acta Astron.* **2022**, *72*, 1–19. [[CrossRef](#)]
18. Turner, J.D.; Flagg, L.; Ridden-Harper, A.; Jayawardhana, R. Characterizing the WASP-4 System with TESS and Radial Velocity Data: Constraints on the Cause of the Hot Jupiter’s Changing Orbit and Evidence of an Outer Planet. *Astron. J.* **2022**, *163*, 281. [[CrossRef](#)]
19. Harre, J.V.; Smith, A.M.S.; Barros, S.C.C.; Boué, G.; Csizmadia, S.; Ehrenreich, D.; Florén, H.G.; Fortier, A.; Maxted, P.F.L.; Hooton, M.J.; et al. Examining the orbital decay targets KELT-9 b, KELT-16 b, and WASP-4b, and the transit-timing variations of HD 97658 b. *Astron. Astrophys.* **2023**, *669*, A124. [[CrossRef](#)]
20. Kokori, A.; Tsirias, A.; Edwards, B.; Rocchetto, M.; Tinetti, G.; Bewersdorff, L.; Jongen, Y.; Lekkas, G.; Pantelidou, G.; Poultourtzidis, E.; et al. ExoClock Project. II. A Large-scale Integrated Study with 180 Updated Exoplanet Ephemerides. *Astrophys. J. Suppl.* **2022**, *258*, 40. [[CrossRef](#)]
21. Benz, W.; Broeg, C.; Fortier, A.; Rando, N.; Beck, T.; Beck, M.; Queloz, D.; Ehrenreich, D.; Maxted, P.F.L.; Isaak, K.G.; et al. The CHEOPS mission. *Exp. Astron.* **2021**, *51*, 109–151. [[CrossRef](#)]
22. Cáceres, C.; Ivanov, V.D.; Minniti, D.; Burrows, A.; Selman, F.; Melo, C.; Naef, D.; Mason, E.; Pietrzynski, G. A ground-based K_s-band detection of the thermal emission from the transiting exoplanet WASP-4b. *Astron. Astrophys.* **2011**, *530*, A5. [[CrossRef](#)]
23. Beerer, I.M.; Knutson, H.A.; Burrows, A.; Fortney, J.J.; Agol, E.; Charbonneau, D.; Cowan, N.B.; Deming, D.; Desert, J.M.; Langton, J.; et al. Secondary Eclipse Photometry of WASP-4b with Warm Spitzer. *Astrophys. J.* **2011**, *727*, 23. [[CrossRef](#)]
24. Zhou, G.; Bayliss, D.D.R.; Kedziora-Chudczer, L.; Tinney, C.G.; Bailey, J.; Salter, G.; Rodriguez, J. Secondary eclipse observations for seven hot-Jupiters from the Anglo-Australian Telescope. *Mon. Not. RAS* **2015**, *454*, 3002–3019. [[CrossRef](#)]
25. Jenkins, J.M.; Twicken, J.D.; McCauliff, S.; Campbell, J.; Sanderfer, D.; Lung, D.; Mansouri-Samani, M.; Girouard, F.; Tenenbaum, P.; Klaus, T.; et al. The TESS science processing operations center. In Proceedings of the Software and Cyberinfrastructure for Astronomy IV, Edinburgh, UK, 26 June–1 July 2016; Chiozzi, G., Guzman, J.C., Eds.; Society of Photo-Optical Instrumentation Engineers (SPIE) Conference Series; SPIE 2016; Volume 9913, p. 99133E. [[CrossRef](#)]

26. Csizmadia, S. The Transit and Light Curve Modeller. *Mon. Not. RAS* **2020**, *496*, 4442–4467. [[CrossRef](#)]
27. Goldreich, P.; Soter, S. Q in the Solar System. *Icarus* **1966**, *5*, 375–389. [[CrossRef](#)]
28. Hoyer, S.; López-Morales, M.; Rojo, P.; Nascimbeni, V.; Hidalgo, S.; Astudillo-Defru, N.; Concha, F.; Contreras, Y.; Servajean, E.; Hinse, T.C. TraMoS project—III. Improved physical parameters, timing analysis and starspot modelling of the WASP-4b exoplanet system from 38 transit observations. *Mon. Not. RAS* **2013**, *434*, 46–58. [[CrossRef](#)]
29. Giménez, A.; Bastero, M. A Revision of the Ephemeris-Curve Equations for Eclipsing Binaries with Apical Motion. *Astrophys. Space Sci.* **1995**, *226*, 99–107. [[CrossRef](#)]
30. Foreman-Mackey, D.; Hogg, D.W.; Lang, D.; Goodman, J. emcee: The MCMC Hammer. *Publ. ASP* **2013**, *125*, 306. [[CrossRef](#)]
31. Schneider, J. Light-Time Effect and Exoplanets. In Proceedings of the The Light-Time Effect in Astrophysics: Causes and Cures of the O-C Diagram, Brussels, Belgium, 19–22 July 2004; Sterken, C., Ed.; Astronomical Society of the Pacific Conference Series; ASP 2005; Volume 335, p. 191.
32. Rein, H.; Liu, S.F. REBOUND: An open-source multi-purpose N-body code for collisional dynamics. *Astron. Astrophys.* **2012**, *537*, A128. [[CrossRef](#)]
33. Ivshina, E.S.; Winn, J.N. TESS Transit Timing of Hundreds of Hot Jupiters. *Astrophys. J. Suppl.* **2022**, *259*, 62. [[CrossRef](#)]
34. Naoz, S.; Farr, W.M.; Lithwick, Y.; Rasio, F.A.; Teyssandier, J. Hot Jupiters from secular planet-planet interactions. *Nature* **2011**, *473*, 187–189. [[CrossRef](#)]
35. Dawson, R.I.; Johnson, J.A. Origins of Hot Jupiters. *Annu. Rev. Astron Astrophys.* **2018**, *56*, 175–221. [[CrossRef](#)]
36. Grunblatt, S.K.; Saunders, N.; Sun, M.; Chontos, A.; Soares-Furtado, M.; Eisner, N.; Pereira, F.; Komacek, T.; Huber, D.; Collins, K.; et al. TESS Giants Transiting Giants. II. The Hottest Jupiters Orbiting Evolved Stars. *Astron. J.* **2022**, *163*, 120. [[CrossRef](#)]
37. Jackson, B.; Adams, E.; Sandidge, W.; Kreyche, S.; Briggs, J. Variability in the Atmosphere of the Hot Jupiter Kepler-76b. *Astron. J.* **2019**, *157*, 239. [[CrossRef](#)]
38. Scandariato, G.; Singh, V.; Kitzmann, D.; Lendl, M.; Brandeker, A.; Bruno, G.; Bekkelien, A.; Benz, W.; Gutermann, P.; Maxted, P.F.L.; et al. Phase curve and geometric albedo of WASP-43b measured with CHEOPS, TESS, and HST WFC3/UVIS. *Astron. Astrophys.* **2022**, *668*, A17. [[CrossRef](#)]
39. van Sluijs, L.; Birkby, J.L.; Lothringer, J.; Lee, E.K.H.; Crossfield, I.J.M.; Parmentier, V.; Brogi, M.; Kulesa, C.; McCarthy, D.; Charbonneau, D. Carbon monoxide emission lines reveal an inverted atmosphere in the ultra hot Jupiter WASP-33 b consistent with an eastward hot spot. *Mon. Not. RAS* **2023**, *522*, 2145–2170. [[CrossRef](#)]
40. Shi, Y.; Wang, W.; Zhao, G.; Zhai, M.; Chen, G.; Jiang, Z.; Ouyang, Q.; Henning, T.; Zhao, J.; Crouzet, N.; et al. Thermal emission from the hot Jupiter WASP-103 b in J and Ks bands. *Mon. Not. RAS* **2023**, *522*, 1491–1503. [[CrossRef](#)]
41. Hoyer, S.; Jenkins, J.S.; Parmentier, V.; Deleuil, M.; Scandariato, G.; Wilson, T.G.; Díaz, M.R.; Crossfield, I.J.M.; Dragomir, D.; Kataria, T.; et al. The extremely high albedo of LTT 9779 b revealed by CHEOPS. An ultrahot Neptune with a highly metallic atmosphere. *Astron. Astrophys.* **2023**, *675*, A81. [[CrossRef](#)]
42. Rauer, H.; Catala, C.; Aerts, C.; Appourchaux, T.; Benz, W.; Brandeker, A.; Christensen-Dalsgaard, J.; Deleuil, M.; Gizon, L.; Goupil, M.J.; et al. The PLATO 2.0 mission. *Exp. Astron.* **2014**, *38*, 249–330. [[CrossRef](#)]
43. Gaia Collaboration.; Prusti, T.; de Bruijne, J.H.J.; Brown, A.G.A.; Vallenari, A.; Babusiaux, C.; Bailer-Jones, C.A.L.; Bastian, U.; Biermann, M.; Evans, D.W.; et al. The Gaia mission. *Astron. Astrophys.* **2016**, *595*, A1. [[CrossRef](#)]
44. Astropy Collaboration.; Robitaille, T.P.; Tollerud, E.J.; Greenfield, P.; Droettboom, M.; Bray, E.; Aldcroft, T.; Davis, M.; Ginsburg, A.; Price-Whelan, A.M.; et al. Astropy: A community Python package for astronomy. *Astron. Astrophys.* **2013**, *558*, A33. [[CrossRef](#)]
45. Astropy Collaboration.; Price-Whelan, A.M.; Sipőcz, B.M.; Günther, H.M.; Lim, P.L.; Crawford, S.M.; Conseil, S.; Shupe, D.L.; Craig, M.W.; Dencheva, N.; et al. The Astropy Project: Building an Open-science Project and Status of the v2.0 Core Package. *Astron. J.* **2018**, *156*, 123. [[CrossRef](#)]
46. Astropy Collaboration.; Price-Whelan, A.M.; Lim, P.L.; Earl, N.; Starkman, N.; Bradley, L.; Shupe, D.L.; Patil, A.A.; Corrales, L.; Basseur, C.E.; et al. The Astropy Project: Sustaining and Growing a Community-oriented Open-source Project and the Latest Major Release (v5.0) of the Core Package. *Astrophys. J.* **2022**, *935*, 167. [[CrossRef](#)]

Disclaimer/Publisher’s Note: The statements, opinions and data contained in all publications are solely those of the individual author(s) and contributor(s) and not of MDPI and/or the editor(s). MDPI and/or the editor(s) disclaim responsibility for any injury to people or property resulting from any ideas, methods, instructions or products referred to in the content.